THE JOURNAL OF PHYSICAL CHEMISTRY B

Article

pubs.acs.org/JPCB

Insights into Structural Properties of Denatured Human Prion 121-230 at Melting Temperature Studied by Replica Exchange Molecular Dynamics

Jaw-Luen Tang,[†] Po-Jen Wu,[‡] Shing-Chuen Wang,[‡] and Cheng-I Lee*[,‡]

[†]Department of Physics, [‡]Department of Life Science, National Chung Cheng University, Ming-Hsiung Chia-Yi, Taiwan 62102, ROC

ABSTRACT: Misfolding and aggregation of the prion protein (PrP) is responsible for the development of fatal transmissible neurodegenerative diseases. PrP undergoes structural conversion from a natively folded state into a misfolded state, resulting in aggregated amyloid fibrils. Partial unfolding has been recognized as an essential step in fibrillation, especially at the middle point of unfolding. To study the possible aggregation-prone states, we characterized the structure of the C-terminal globular domain of human prion (huPrP) 121-230 near extended conformation at melting temperature by replica exchange molecular dynamics (REMD) simulation, as the REMD method is the most suited generalized-ensemble algorithm that performs random walk in energy space and promotes a system to escape from local energy traps. Our results revealed that denatured huPrP is partially folded with α-helical structure at melting temperature. The simulation results provide further insight into the unfolding of prion, which is essential in pathogenesis of prion diseases.

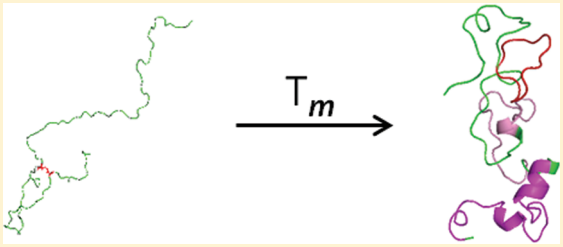

INTRODUCTION

Prion proteins (PrPs) are infectious pathogens of a group of fatal neurodegenerative diseases in mammals known as transmissible spongiform encephalopathies (TSEs).[1] TSEs have been attributed to the structural conversion of prion. The normal, cellular form of PrP (PrP^{C}) is rich in α-helix structures, whereas the abnormal and infectious Scrapie isoform of PrP (PrP^{Sc}) has a pronounced tendency to misfold and to aggregate subsequently into highly stable and insoluble plaques rich in β-sheet structures. The structure of PrP^{Sc} and the mechanism of its formation have yet to be fully elucidated.

In previous studies of PrP, a partially folded intermediate of PrP 90-231 has been suggested.[2−4] These partially unfolded transient intermediate states can potentially initiate amyloid formation[5,6] under kinetic control[7] and in accordance with the nucleation polymerization model.[8] The strong correlation between unfolding and fibrillation emphasizes the importance of unfolded states.[2]

The role of unfolded states in fibril formation has been implicated in previous studies. In the study of Baskakov, wherein recombinant PrP was studied in the presence of urea, the shortest lag phase for fibril conversion was observed at partially denaturing conditions, near the concentration of urea corresponding to the middle point of unfolding.[9] Consequently, further insight into the structure of unfolded PrP, especially at the middle point of unfolding, is important to understanding amyloid fibril formation.

The middle point of unfolded states is represented by structures at the melting temperature in temperature-induced denaturation. The unfolded states are thermodynamically distinct from the native state, but unfolded states might preserve some of the structural features observed in the native state. The structural features of unfolded huPrP at melting temperature are critical in the mechanism analysis of PrP^{Sc} formation. Therefore, in addition to understanding the folded structure, further understanding of unfolded states and, in particular, of unfolded states in intermediate PrP^{Sc}, is essential.

Experimental observation has indicated that PrP fibril is rich in cross β-sheet structure.[10] This observation has led to the interpretation that the helical PrP protein changed to β-structure before polymerization into amyloid fibrils. Previous studies in several groups indicated that the folded α-helical PrP undergoes a three-state, chemical-induced, or temperature-induced unfolding process under acidic condition, and that this unfolding results an apparent equilibrium intermediate with a β-sheet-rich conformation.[11−13] Later studies exhibited a two-state transition converting α-helical PrP into unfolded β-sheet intermediate at low pH.[14,15] Detailed characterization of the denaturation pathway done by Baskakov et al. revealed that the β-sheet-rich isoform is formed only upon the oligomerization of PrP rather than an equilibrium intermediate in the unfolding of PrP.[7,16] They clearly pointed out that both the native and denatured species gradually increases with denaturants.[9] DeMarco and Daggett have simulated structural conversion of prion and they demonstrated a very small difference between native structure at neutral pH and the PrP^{Sc}-like structure at low pH.[15] In addition to the highly conserved α-helix simulated in the PrP^{Sc}-like structure, three-stranded sheet and an isolated strand are formed in the core of the β-sheet.[15] Overall, these

Received: September 1, 2011
Revised: December 20, 2011
Published: February 16, 2012

conflicting results keep the structural feature of the PrP intermediate ambiguous.

In this study, the population of the secondary structure of the partially unfolded huPrP at melting temperature near extended conformation with full atomic details using replica exchange molecular dynamics (REMD) simulation was investigated. The REMD method was originally introduced by Sugita and Okamoto.[17] REMD combines the idea of multiple-copy simulation, simulated annealing, and Monte Carlo methods.[18,19] REMD is the generalized-ensemble algorithm most suited for this study as it performs random walk in energy space at different temperatures, promoting a system to escape from local energy traps to explore new conformational space. REMD was designed to enhance the sampling efficiency. Delightfully, a single REMD simulation can give thermodynamic quantities at a range of temperatures. In comparison to conventional MD, REMD can sample more conformational space within the same time scale.[20]

In this work, we primarily characterized the structure and heat-induced denaturation of huPrP 23−230 and huPrP 121-230 by circular dichrosim (CD) spectroscopy since previous NMR studies reported structured region in residues 125−228 and flexible N-terminal fragment.[15] As huPrP 23−230 and huPrP 121-230 have the same structure and melting point, simulation results of huPrP 121-230 can represent the structural features of full-length huPrP. Subsequently, the conformation free energy surface of the C-terminal domain of huPrP 121-230 with full atomic details of the protein and the implicit solvent using REMD was simulated. In total, 24 replicas of all-atom simulations of huPrP starting from an extended conformation were conducted. The melting temperature of huPrP was determined experimentally by heat-induced denaturation of α-helix in huPrP monitored by CD spectroscopy.

MD simulation of protein folding can easily produce millions of sets of coordinates. Clustering is a general data-mining method applied to any collection of data points where a function measuring distance between pairs of points is available. Half unfolded states can be categorized through such a clustering method. The structures within one cluster are ideally more similar to each other than to the structures from other clusters. From clustering analysis, the most populated structure can be determined. Details of the half unfolded states were investigated and are discussed herein.

METHODS

Expression and Purification of Human Prion Proteins. Plasmids pRSET-A encoding huPrP 23-230 and huPrP 121-230 are kindly gifts from Professor Kurt Wüthrich. Each plasmid was transformed into competent *E. coli* BL21 (DE3), and huPrP proteins were expressed by induction with isopropyl β-D-galactopyranoside. The purification was based on the procedures developed by the Wüthrich group.[21] The purity of the isolated protein was confirmed by SDS-PAGE. The correct native conformation, containing mainly α-helical structures, was confirmed by circular dichroism spectroscopy.

Circular Dichroism Spectroscopy. CD spectrum of huPrP was recorded with a Jasco J-815 spectrometer. For measurements in the far-UV region, a quartz cell with a path length of 0.1 cm was used under nitrogen atmosphere. The concentration of huPrP was kept constant at 10 μM in 10 mM MES (pH 7.0). An accumulation of five scans with a scan speed of 50 nm per minute was performed at 20 °C. The heat-induced denaturation of huPrP was conducted at the rate of 1 °C/min, and the ellipticity at 222 nm was collected every 0.5 °C.

Simulation Procedure. Twenty four replicas of REMD simulations of huPrP starting from an extended conformation were conducted. These replicas developed independently over a range of temperatures. The independent replicas at different temperatures can exchange between neighboring replicas at the fixed time intervals with a transition probability satisfying the detailed balance. The replicas exchange on the basis of the Metropolis criterion with an acceptance probability defined by the following equation:[17]

$$P(1 \leftrightarrow 2) = \min\left(1, \exp\left[\left(\frac{1}{K_B T_1} - \frac{1}{K_B T_2}\right)(U_1 - U_2)\right]\right) \quad (1)$$

where $P(1\leftrightarrow2)$ is the exchange probability, K_B is Boltzmann's constant, U_1 and U_2 are the instantaneous potential energies, and T_1 and T_2 are the reference temperatures. This equation is well-suited for the canonical ensemble, and works for systems that have small volumetric fluctuations. The all-atom simulation described herein satisfies this requirement.

In this work, the temperature setting used for sheep PrP 125-230 such that MD simulations were exchanged at 320.0, 322.0, 324.0, 326.0, 328.1, 330.2, 332.3, 334.4, 336.5, 338.6, 340.8, 343.0, 345.2, 347.4, 349.6, 351.8, 354.0, 356.2, 358.5, 360.8, 363.1, 365.4, 367.7, and 370.0 K was used.[22] All of the replicas were equilibrated for 20 ns without exchanging temperatures and then extended for 65 ns of REMD simulation. The generalized Born model used in this study modified the calculation of Born radii and improved the accuracy in the solvent polarization for macromolecules.[23] The combinational use of the all-atom point-charge force-field (also known as ff03[24]) and the generalized Born model led to successful folding of several proteins.[25] The AMBER 11 simulation package[26] was used in both REMD simulation and data analysis.

The melted huPrP 121-230 was computed starting from an extended huPrP. To generate the initial extended structure, a heating method was applied to a known NMR structure (PDB code 1hjn,[15] Figure 1A), enabling it to unfold at 600 K for 40 ns of MD simulation to result in an extended conformation (Figure 1B) as described previously.[27] During this simulation, the disulfide covalent bond between residues 179 and 214 was preserved. In total, 24 replicas with duration of 65 ns and with an integration time step of 2 fs were computed based on the extended huPrP with different random number seeds to generate the initial conditions. A 16 Å force-shifted nonbonded

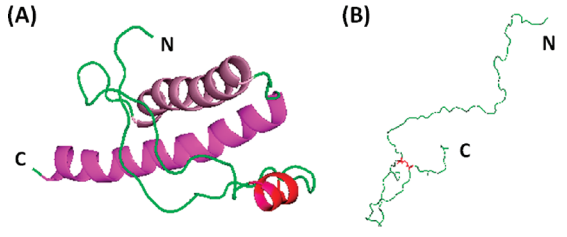

Figure 1. (A) NMR structure of huPrP121-231 (PDB, 1hjn[15]); the helix regions I, II, and II are colored in red, pink, and magenta, respectively. (B) Fully unfolded huPrP 121-230 at 600 K with the disulfide-bond shown in red.

cutoff and generalized Born solvent models with salt concentration of 0.2 M were applied.[23]

Structural Analysis. The structural information of the unfolded human prion 121-230 can be illustrated as root-mean-square deviation (rmsd) of C^{α}. Rmsd of C^{α} was calculated based on residues 126-227. The terminal residues in the N- and C-terminus were excluded due to their high flexibility. The information of the secondary structure was represented by the fraction of α-helices (helicity) and antiparallel β-strands. According to the NMR structure,[15] native huPrP contains three helices: helices I (residues 144−156), II (residues 173−194), and III (residues 200−227) as defined by calculation with a DSSP algorithm.[28] Helicity over 65 ns of simulation was calculated based on the number of helical residues in the helix region in the denatured state as compared to that in the native state. The helicity of the entire huPrP was determined from residues 125−228. The calculation of helicity can be expressed as:

$$\text{helicity} = (\text{no. of helix residues})/(\text{no. of residues in the entire protein or in helix region})$$

Similarly, the fraction of antiparallel β-strand content was calculated. Two antiparallel β-strand regions were defined from the native structure at residues 129−133 (β-strand I) and 160−163 (β-strand II). The fraction of antiparallel β-strand content was calculated according to the following formula:

$$(\text{no. of antiparallel } \beta\text{-strand residues})/(\text{no. of residues in the entire protein or in antiparallel } \beta\text{-strand residues})$$

Clustering Analysis. The cluster-to-cluster distance is defined as the average of all distances between individual points of two clusters according to the so-called average-linkage algorithm. The average-linkage algorithm is one of the best clustering methods as suggested by Shao et al.[29] Simulated trajectories were clustered into distinct groups based on average linkage methods by *ptraj*. Based on the main-chain rmsd, each snapshot is compared against the average coordinates of the existing groups after rigid-body alignment. A snapshot may become a member of its closest cluster if the rmsd is smaller than a given cutoff (3 Å). Otherwise, a new cluster would be generated if the minimum rmsd exceeded the cutoff.

RESULTS

Full length huPrP is a 210-residue protein. A previous NMR study revealed that huPrP proteins contain a globular domain that extends approximately from residues 125−228.[30] The N-terminal fragment of huPrP is flexibly disordered. The globular domain contains one two-stranded antiparallel β-bridge and three α-helices as shown in Figure 1A (PDB code: 1hjn[15]). The high content of α-helical structure in huPrP 121-230 was characterized as a comparison to huPrP 23-230 in the CD spectrum as illustrated in Figure 2A. The secondary structure of huPrP 121-230 is extremely similar to huPrP 23-230, while the molar ellipticity of huPrP 23-230 is weaker than the ellipticity in huPrP 121-230 because of unstructured N-terminal fragment.

PrP is known to be a highly stable protein, and therefore, a high value of melting temperature is expected. Heat-induced denaturation of huPrP was monitored by the change of ellipticity at 222 nm. The result of heat-induced denaturation

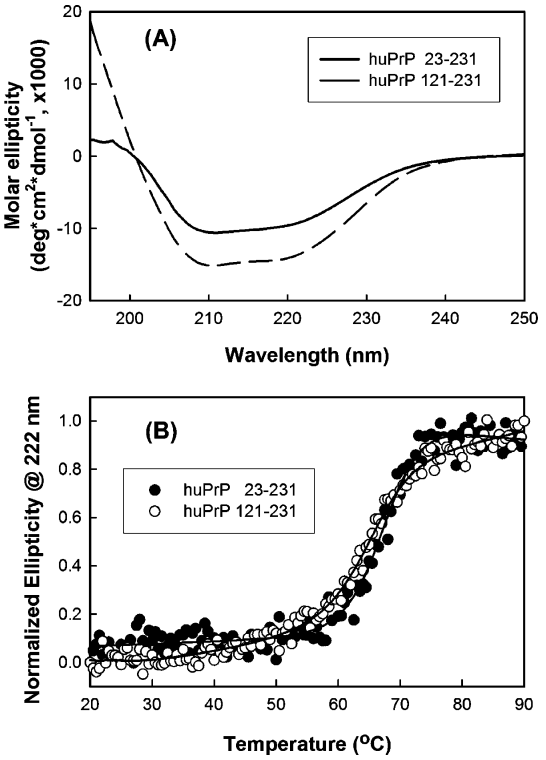

Figure 2. (A) Spectrum of native huPrP at 20 °C. (B) The heat-induced denaturation of huPrP recorded with the change of ellipticity at 222 nm.

(Figure 2B) was analyzed using the Gibbs−Helmholtz equation:

$$\Delta G_{\mathrm{U}}^{\circ}(T) = \Delta H^{\circ}(T_{\mathrm{m}})\left(1 - \frac{T}{T_{\mathrm{m}}}\right) - \Delta G_{\mathrm{p}}^{\circ}\left[(T_{\mathrm{m}} - T) + T\ln\left(\frac{T}{T_{\mathrm{m}}}\right)\right] \quad (2)$$

Based on the above equation, the melting temperature (T_{m}) of huPrP 23−230 and 121-230 was determined to be 67.7 (340.8 K) and 66.9 °C (340.0 K), respectively, at pH 7.0. This value is consistent with previous study on mouse PrP 23-230 (66.7 °C)[31] and sheep PrP (~70.3 °C).[32] This thermal-induced protein denaturation experiment clearly determined the melting temperature for further simulation.

These CD results indicated that huPrP 23-230 and huPrP 121-230 have the same structure and thermal-stability, the following structural analysis of huPrP 121-230 at melting-point can represent the structural information of full-length huPrP.

Experimental studies indicated that impairing the native protein structure is essential in fibril formation since the structural conversion of PrP protein into PrP fibrils requires denaturants.[16] The rmsd and the secondary structure feature of the partially unfolded prion have not been determined experimentally. To gain further insight into the unfolded state at melting temperature, computer simulation is the best solution. Therefore, we designed the extended structure as the starting structure to be compared with as described previously.[27] In this starting structure, huPrP is an extended conformation and lacks all characteristics of the secondary structure (Figure 1B). The disulfide-bond between residues 179 and 214 was preserved during high-temperature simulation

dx.doi.org/10.1021/jp208433w | J. Phys. Chem. B 2012, 116, 3305−3312

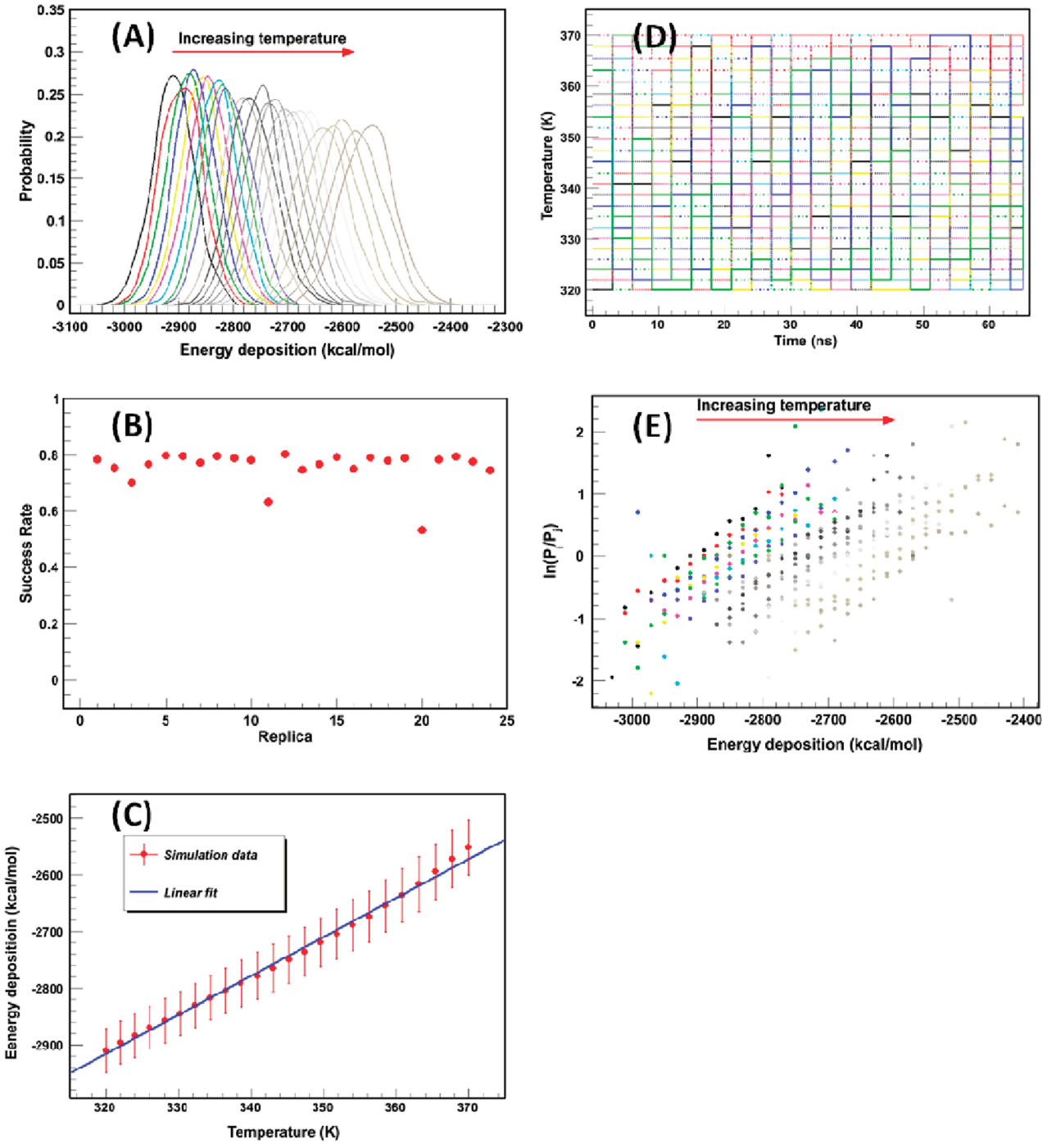

Figure 3. (A) Potential energy distributions between neighboring replicas. (B) Average success rates of 24 replicas. (C) Average potential energy of 24 replicas. (D) Exchanges of replicas in the temperature space; temperatures of odd-numbered replicas are shown. (E) Energy population ratios for overlap between adjacent temperatures.

since previous studies indicated the existence of disulfide bonds during misfolding of PrP.[33,34] This extended structure was optimized by local energy minimization prior to the following REMD simulations.

Replica Exchange Molecular Dynamics. This REMD simulation includes 24 replicas with temperature ranging from 320 to 370 K to across the melting temperature at 340.8 K. The potential energy distributions between neighboring replicas are shown in Figure 3A. Highly overlapped potential energy distributions lead to high success exchange rate at ~78% over the entire temperature range as indicated in Figure 3B. The values of mean potential energy of 24 replicas are reported in Figure 3C. The mean potential energy increases linearly along the input temperature values. The exchanges in the temperature space recorded from the end of each nanosecond are illustrated in Figure 3D. All trajectories visit nearly all temperature levels between 320 and 370 K within the simulation time. The desired sampling over the potential energy space was verified by the ratio of the potential energy distributions of the adjacent temperatures as revealed in Figure 3E. When the potential

dx.doi.org/10.1021/jp208433w | J. Phys. Chem. B 2012, 116, 3305–3312

energy distribution functions $P(E; T_i)$ and $P(E; T_j)$ follow the Boltzmann distribution, their ratios satisfy eq 3

$$\ln\left(\frac{P(E;\ T_i)}{P(E;\ T_j)}\right) = \frac{1}{k_B}\left(\frac{1}{T_j} - \frac{1}{T_i}\right)E + \text{constant} \quad (3)$$

The plot of this ratio is shown in Figure 3E. Linearity is observed in all replicas, suggesting that the configurations from our simulation follow the Boltzmann distribution.

Thermodyanmic Analysis. Assuming a two-state thermodynamic model with only denatured state and the general folded state, the melting temperature can also be obtained from the REMD simulation using the population of denatured state and van't Hoff analysis.[35−37] Since heat capacity is a direct measure of the thermodynamic properties in protein folding and melting transition can be deduced from its profile, we have performed a calculation on heat capacity profile in the temperature range of 320−360 K from the energy variances based on two data sets: 0−30 ns and 30−60 ns. Heat capacity was computed at each temperature by $C_p = (\langle E^2\rangle - \langle E\rangle^2)/RT^2$, where E is the energy, R is the gas constant, and T is the temperature. As shown in Figure 4, the resulting heat capacity

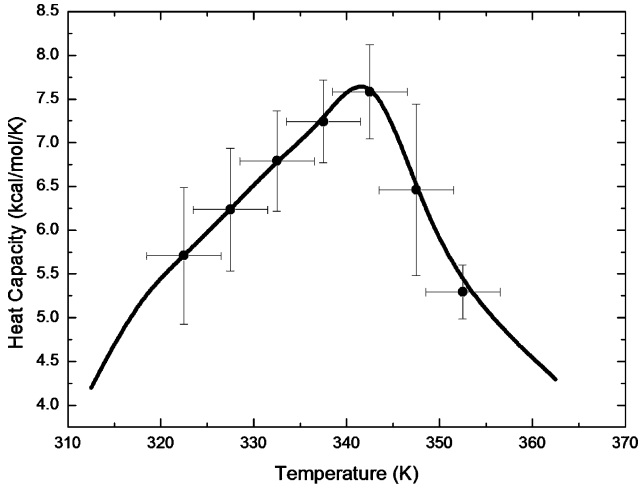

Figure 4. Heat capacity as a function of temperature. The mean values (dots) and error bars were obtained by dividing data into two sets for analysis: 0−30 ns and 30−60 ns. The solid line is used for eye-guiding only.

profile exhibits one broad structure at around 342 K, indicative of one distinct melting transition. The melting temperature was estimated to be T_m = 342 ± 5 K, in close agreement with the experimental one (T_m = 340.8 K). The close T_m values determined by the experiment and the simulation indicate that the force field and the REMD parameters used in this study are appropriate.

Analysis of rmsd of C^α. To quantitatively evaluate the structural similarity over the simulation time as compared to the native huPrP structure, rmsd of C^α was calculated for the globular structured region (residues 126−227). Overall, as shown in Figure 5A, the rmsd of C^α in the entire simulated protein increases slightly with some fluctuations with increasing time. To look closely at the structural detail, we calculated rmsd of C^α in the β-strand I, β-strand II and helices I, II and III based on the structural feature in the native huPrP structure. In the β-strand regions, rmsd of C^α increases slightly in β-strand I (Figure 5B), and remains nearly constant in β-strand II (Figure

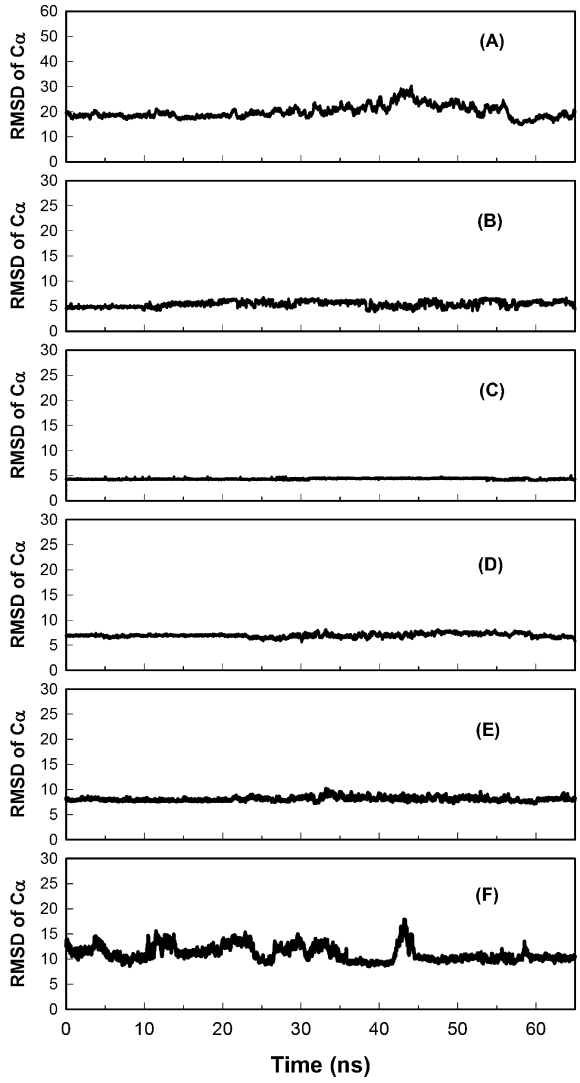

Figure 5. At melting temperature, rmsd of C^α in (A) the entire hPrP, (B) β-strand I, (C) β-strand II, (D) helix I, (E) helix II, and (F) helix III regions. The antiparallel and helical regions are defined based on the native structure.

5C). In the helix regions, regions I and II (Figure 5, panels D and E, respectively) perform similarly that rmsd of C^α remain almost constant. Dramatically, rmsd of C^α in helix III fluctuates over the range of ∼8 Å (Figure 5F). Overall, the structure change in helix III is pronounced, but the changes in other regions are not significant.

Analysis of α-Helicity of Native Helical Regions. Since the native structure of the simulated protein contains three helices, the development of the helical structure would be a good measure of the folding process. Therefore, the average of the fraction of the α-helices (helicity) of denatured huPrP was considered. In the entire protein, denatured huPrP still exhibit helical features at 0.164. We further calculated the helicity of helix regions I−III in the denatured state as listed in Table 1. In helix I, the helix feature is completely lost so that the helicity of helix I is zero. In helix II, the helicity fluctuates between 0.133 and 0.265. In helix III, the helicity fluctuates between 0.208 and 0.448. Notably, all the helicity values in helix III are higher than the helicity in the entire protein at 0.164. This high helicity indicates high content of helical structure in helix III in the denatured state of huPrP in the middle point of unfolding.

dx.doi.org/10.1021/jp208433w | J. Phys. Chem. B 2012, 116, 3305−3312

Table 1. Structural Features of huPrP at Melting Temperature

protein region	helicity
entire protein	0.164 ± 0.044
helix I[a]	0.000 ± 0.006
helix II[a]	0.199 ± 0.066
helix III[a]	0.328 ± 0.120
protein region	fraction of antiparallel β-strand
entire protein	0.042 ± 0.017
β-strand I[a]	0.002 ± 0.007
β-strand II[a]	0.001 ± 0.004

[a]The helical and antiparallel regions are defined based on the native structure.

Analysis of Antiparallel β-Strand. The significance of the formation of antiparallel β-strand structure in amyloid proteins is that amyloid fibrils are rich in antiparallel β-strand structures. Therefore, we analyzed the degree of antiparallel β-strand content using the same method as used previously for determining helicity. The fraction of antiparallel β-strand is extremely low at 0.025−0.059. The contents of antiparallel β-strand structure in β-strand I and β-strand II are much lower than the content in the entire protein. Overall, the denatured state of huPrP at the melting temperature does not have distinct β-strand features.

Time-Course of the Secondary Structural Features. The features of the secondary structure of huPrP in the course of simulation time at melting temperature are represented in Figure 6. It is clear that the C-terminal domain is rich with α-helical structures along the simulation, especially in helix III. Consistent with helicity analysis, the helix I region (residues 144−156) does not show any helical structure in the entire simulation. Antiparallel β-strand are shown in the N-terminus, but this feature diminishes gradually after 25 ns, while turns are the major secondary structure. Interestingly, some of the antiparallel β-strands are shown in the helix I region. The population of the secondary structure in the entire simulation was analyzed and data shown in Figure 7. Overall, half of the huPrP 125-228 is structured in the middle point of unfolding. About 26% of the snapshots have features of α-helix and 3−10-helix. Only 4% of the snapshots show features of antiparallel β-strands.

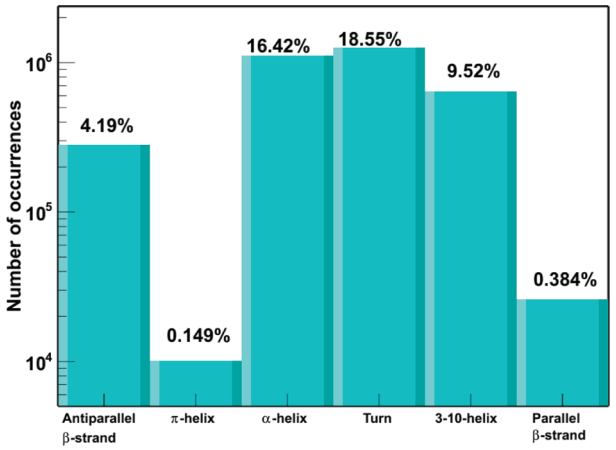

Figure 7. Distribution of various features of secondary structural in the entire MD simulation at melting temperature.

Clustering Analysis. The 24 most populated clusters occupy 25% of the analyzed snapshots, and the secondary structure properties of these clusters were analyzed. In these 24 represented structures, α-helical structure in helix I is lost in all of them, but in most of them, helical content in helix II and helix III is preserved. In the 24 most populated structures, 21 of these structures have α-helical content in both helices II and III, and three of the structures have α-helical content only in helix III. The three most populated structures are illustrated in Figure 8. Clearly, α-helical structures are mostly formed in helix III (magenta ribbons in Figure 8) and some in helix II (pink ribbons in Figure 8). Besides helical regions in the native PrP structure, small fragments of α-helices are observed in the N-terminal domain of the most populated structure (Figure 8A) and the adjunction of helix II and helix III in three most populated structures (Figure 8). Notably, three residues in helix I are identified as β-strands in most of the analyzed populated structures.

DISCUSSION

In conventional protein-folding simulations, it is difficult to obtain accurate canonical distributions at low temperatures since the simulations tend to get trapped in the local minimum-energy states. Generalized-ensemble algorithm was developed to induce random walk in energy space and to allow the

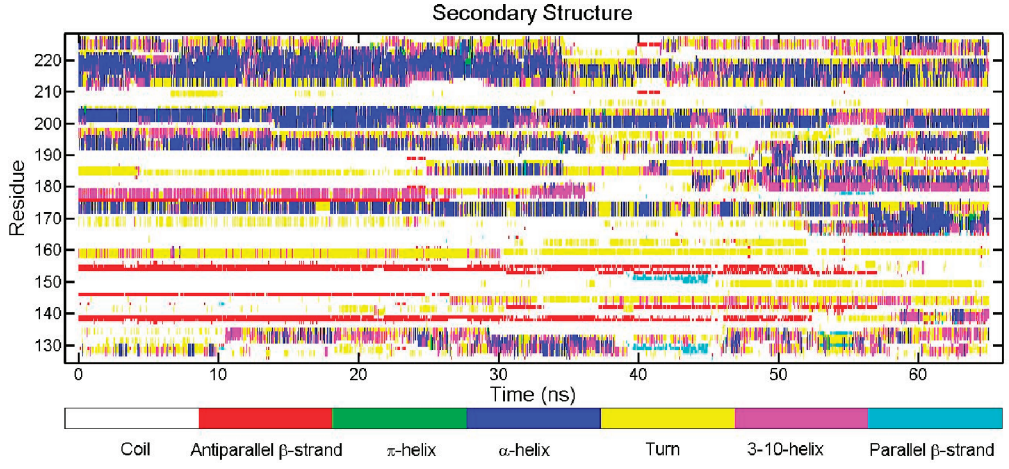

Figure 6. Change of the secondary structure at melting temperature.

dx.doi.org/10.1021/jp208433w | J. Phys. Chem. B 2012, 116, 3305−3312

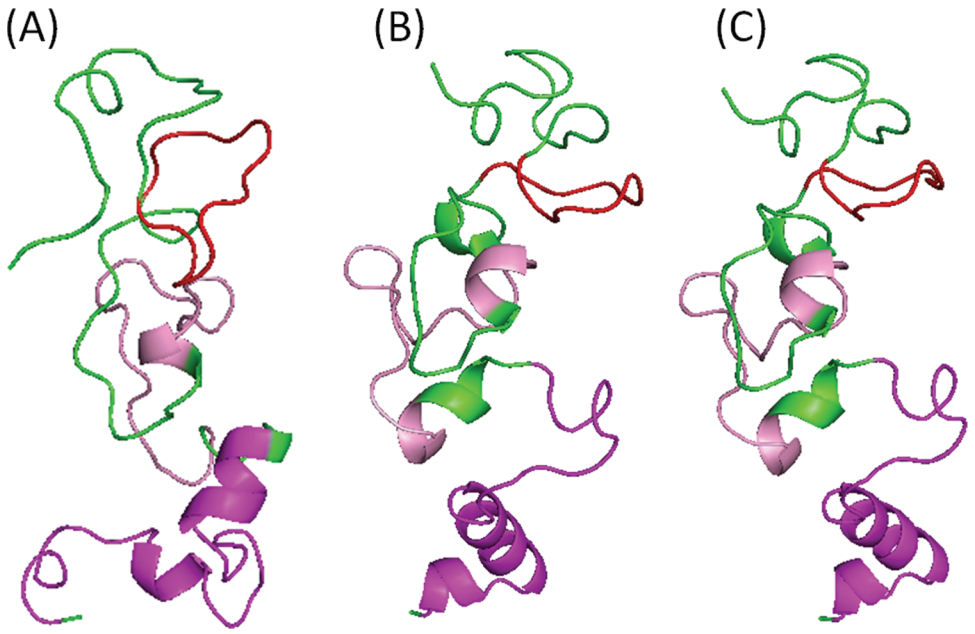

Figure 8. Based on the clustering analysis, (A) the most populated (B) second populated and (C) the third populated structures. The helix regions I, II, and III in the native states are colored in red, pink and magenta, respectively.

simulations to escape from local minima-energy states.[38] Later, Sugita and Okamoto developed an efficient molecular dynamics algorithm known as REMD.[17] REMD is the most suitable generalized-ensemble algorithm for the study of unfolded states as it performs random walk in energy space at different temperatures and promotes a system to escape from local energy traps to explore new conformational space.

The formation of amyloid fibrils by the recombinant PrP has been studied in the presence of urea.[9] The shortest lag phase for fibril conversion was observed at partially denaturing conditions, close to the concentration of urea corresponding to the middle point of unfolding. Prior to studying amyloid fibrils, it is essential to gain further insight into the structure of unfolded PrP at the middle point of unfolding. In the temperature-space, the structures at melting point represent the middle point of unfolded states. Therefore, we are interested in the structure of PrP at melting temperature. The melting temperature was determined experimentally at 67.7 °C (340.8 K) and at 342 ± 5 K from REMD simulation.

In this study, we focused on the structure of huPrP at middle point of unfolding, the state that PrP forms fibrils readily. Overall, the structure of denatured huPrP is deviated significantly from the natively folded structure with rmsd of C^{α} in the entire proteins at ~20 Å. We found that the helical structure is completely lost in helix I, but mostly preserved in helix II and helix III. Three residues are identified as β-strand in helix I region, but the fraction of antiparallel β-strand is lower than 25% in this region. It is difficult to quantify formation of antiparallel β-sheet based on just a few β-strand residues. Furthermore, an H/D exchange study on huPrP fibrils suggests that β-structure is highly unlikely to arise from N-terminal fragment to residue ~169.[39] Therefore, the few residues identified as β-strand in the helix I region might not have direct impact on fibril formation.

As β-sheet-rich structure was observed in PrP fibrils,[10] and the β-structure is formed easily upon partially unfolding of native PrP. The structural feature of PrP intermediates has to be clarified. Previous studies proposing formation of β-sheet-rich structures in the intermediate state.[11−15,40] In contrast, our simulation demonstrates a partially folded α-helical structure with extremely low fraction of β-strand in 65 ns of simulation. The little fraction of β-strand is significantly different from the modeling result of DeMarco and Daggett that PrP^{Sc}-like structure preserved most of α-helical conformation with additional formation of β-strands.[15] DeMarco and Daggett performed a traditional MD simulation for 20 ns in which the space phase of sampling is limited, and the represented structure was generated from the 8-ns structure. In their simulation, the rmsd of C^{α} for unfolded structure at low pH is only 5.2 Å. In contrast, we conducted 24 replica of 65-ns simulation with REMD which are powerful in searching new conformational space, and the most populated structure was analyzed by clustering among 65-ns of trajectories. The rmsd of C^{α} in the denatured huPrP is ~20 Å. Extensive sampling is critical in the simulation of protein structures, especially in the denatured states. Otherwise, the proteins will be trapped in the local energy minimum resulting similar structures to the native state.

This study of denatured huPrP at melting temperature is comparable to our previous simulation of denatured state of huPrP in the native condition that denatured PrP is partially folded with α-helical structure carrying very little feature of β-strand. These results suggest that PrP gradually changes the structure from highly α-helical structure to partially α-helical conformation upon unfolding. Our simulation result is in contrast of Daggett's modeling result and the proposal of β-sheet-rich intermediates. Instead, our study is consistent with the result of Baskakov et al that β-isoform is oligomeric rather than an equilibrium intermediate in the unfolding of PrP.[7]

This computational simulation illustrates that the denatured state of PrP in the middle point of unfolding preserves part of the α-helical structure observed in the native state. Recent crystal structure study revealed formation of intermolecular β-sheet between PrP dimers near α-helix II.[41] Therefore, we propose that huPrP partially conserves intramolecular helical

feature during the unfolding in order to form intermolecular β-sheet for subsequent amyloid polymerization.

Understanding the structural features of PrP in the intermediates is required to clarify the mechanism of conformational change of PrP into infectious aggregated form. This mechanism of structural conversion is essentially in the development of therapeutic methods. This study illustrates the structure of intermediate state is partially folded α-helix rather than β-sheet-rich structure. As β-rich oligomers are thermodynamically more stable than α-helical PrP monomers,[7] the target of the drug design can be focus on the stable β-oligomers.

CONCLUSION

In this study, the denatured state of huPrP at melting temperature was characterized by REMD. The structural analysis indicated that the most populated denatured state in the middle point of unfolding is partially folded with significant α-helical feature. Therefore, we propose that huPrP conserves intramolecular helical structure, and that the β-sheets observed in amyloid fibrils may be formed from intermolecular interactions rather than intramolecular forces. As huPrP can readily convert to amyloid fibrils in the middle of unfolding, these results provide further insight into the unfolding of prion and possible strategy for drug design.

AUTHOR INFORMATION

Corresponding Author

*E-mail: biocil@ccu.edu.tw. Telephone: 886-5-2720411 #66511. Fax: 886-5-2722871.

ACKNOWLEDGMENTS

We are grateful to the National Center for High-performance Computing for computer time and facilities, and National Science Council for financial support (NSC 99-2321-B-194-002, NSC 100-2321-B-194-001, NSC 96-2112-M-194-004-MY3, and NSC 99-2112-M-194-004-MY3). Usage of PyMol graphics packages is gratefully acknowledged. We also thank Dr. Jyh-Shyon Ho for technical assistance and Dr. Raymond Chung for editing the manuscript.

REFERENCES

(1) Prusiner, S. B. *Proc. Natl. Acad. Sci. U.S.A.* **1998**, *95*, 13363−83.
(2) Apetri, A. C.; Surewicz, K; Surewicz, W. K. *J. Biol. Chem.* **2004**, *279*, 18008−14.
(3) Kuwata, K.; Li, H.; Yamada, H.; Legname, G.; Prusiner, S. B.; Akasaka, K; James, T. L. *Biochemistry* **2002**, *41*, 12277−83.
(4) Nicholson, E. M.; Peterson, R. W; Scholtz, J. M. *J. Mol. Biol.* **2002**, *321*, 355−62.
(5) Abedini, A; Raleigh, D. P. *Phys. Biol.* **2009**, *6*, 15005.
(6) Chiti, F; Dobson, C. M. *Nat. Chem. Biol.* **2009**, *5*, 15−22.
(7) Baskakov, I. V.; Legname, G.; Prusiner, S. B; Cohen, F. E. *J. Biol. Chem.* **2001**, *276*, 19687−19690.
(8) Kelly, J. W. *Curr. Opin. Struct. Biol.* **1998**, *8*, 101−106.
(9) Baskakov, I. V.; Legname, G.; Gryczynski, Z; Prusiner, S. B. *Protein Sci.* **2004**, *13*, 586−595.
(10) Nguyen, J. T.; Inouye, H.; Baldwin, M. A.; Fletterick, R. J.; Cohen, F. E.; Prusiner, S. B; Kirschner, D. A. *J. Mol. Biol.* **1995**, *252*, 412−22.
(11) Swietnicki, W.; Petersen, R.; Gambetti, P; Surewicz, W. K. *J. Biol. Chem.* **1997**, *272*, 27517−20.
(12) Zhang, H.; Stockel, J.; Mehlhorn, I.; Groth, D.; Baldwin, M. A.; Prusiner, S. B.; James, T. L; Cohen, F. E. *Biochemistry* **1997**, *36*, 3543−53.
(13) Hornemann, S; Glockshuber, R. *Proc. Natl. Acad. Sci. U.S.A.* **1998**, *95*, 6010−4.
(14) Rezaei, H.; Choiset, Y.; Eghiaian, F.; Treguer, E.; Mentre, P.; Debey, P.; Grosclaude, J; Haertle, T. *J. Mol. Biol.* **2002**, *322*, 799−814.
(15) Calzolai, L; Zahn, R. *J. Biol. Chem.* **2003**, *278*, 35592−6.
(16) Baskakov, I. V.; Legname, G.; Baldwin, M. A.; Prusiner, S. B; Cohen, F. E. *J. Biol. Chem.* **2002**, *277*, 21140−8.
(17) Sugita, Y; Okamoto, Y. *Chem. Phys. Lett.* **1999**, *314*, 141−151.
(18) Hansmann, U. H. E; Okamoto, Y. *Curr. Opin. Struct. Biol.* **1999**, *9*, 177−183.
(19) Mitsutake, A.; Sugita, Y; Okamoto, Y. *Biopolymers* **2001**, *60*, 96−123.
(20) Sanbonmatsu, K. Y; Garcia, A. E. *Proteins* **2002**, *46*, 225−234.
(21) Zahn, R.; von Schroetter, C; Wuthrich, K. *FEBS Lett.* **1997**, *417*, 400−4.
(22) De Simone, A.; Zagari, A; Derreumaux, P. *Biophys. J.* **2007**, *93*, 1284−92.
(23) Onufriev, A.; Bashford, D; Case, D. A. *Proteins* **2004**, *55*, 383−394.
(24) Duan, Y.; Wu, C.; Chowdhury, S.; Lee, M. C.; Xiong, G. M.; Zhang, W.; Yang, R.; Cieplak, P.; Luo, R.; Lee, T.; et al. *J. Comput. Chem.* **2003**, *24*, 1999−2012.
(25) Lei, H.; Wu, C.; Wang, Z. X.; Zhou, Y; Duan, Y. *J. Chem. Phys.* **2008**, *128*, 235105.
(26) Case, D. A., Darden, T. A., Cheatham, I., T., E., Simmerling, C. L., Wang, J., Duke, R. E., Luo, R., Crowley, M., Walker, R. C., Zhang, W., et al.., *AMBER 11*; University of California: San Francisco, CA, 2010.
(27) Lee, C. I; Chang, N. Y. *Biophys. Chem.* **2010**, *151*, 86−90.
(28) Kabsch, W; Sander, C. *Biopolymers* **1983**, *22*, 2577−637.
(29) Shao, J. Y.; Tanner, S. W.; Thompson, N; Cheatham, T. E. *J. Chem. Theory Comput.* **2007**, *3*, 2312−2334.
(30) Zahn, R.; Liu, A.; Luhrs, T.; Riek, R.; von Schroetter, C.; Lopez Garcia, F.; Billeter, M.; Calzolai, L.; Wider, G; Wuthrich, K. *Proc. Natl. Acad. Sci. U.S.A.* **2000**, *97*, 145−50.
(31) Robinson, P. J; Pinheiro, T. J. T. *Biochemistry* **2009**, *48*, 8551−8558.
(32) Rezaei, H.; Marc, D.; Choiset, Y.; Takahashi, M.; Hoa, G. H. B.; Haertle, T.; Grosclaude, J; Debey, P. *Eur. J. Biochem.* **2000**, *267*, 2833−2839.
(33) Turk, E.; Teplow, D. B.; Hood, L. E; Prusiner, S. B. *Eur. J. Biochem.* **1988**, *176*, 21−30.
(34) Welker, E.; Raymond, L. D.; Scheraga, H. A; Caughey, B. *J. Biol. Chem.* **2002**, *277*, 33477−81.
(35) Becktel, W. J; Schellman, J. A. *Biopolymers* **1987**, *26*, 1859−77.
(36) Lei, H.; Wu, C.; Liu, H; Duan, Y. *Proc. Natl. Acad. Sci. U.S.A.* **2007**, *104*, 4925−30.
(37) Wu, C; Shea, J. E. *PLoS Comput. Biol.* **2010**, *6*, e1000998.
(38) Hansmann, U. H. E; Okamoto, Y. *J. Comput. Chem.* **1997**, *18*, 920−933.
(39) Lu, X.; Wintrode, P. L; Surewicz, W. K. *Proc. Natl. Acad. Sci. U.S.A.* **2007**, *104*, 1510−5.
(40) Morillas, M.; Vanik, D. L; Surewicz, W. K. *Biochemistry* **2001**, *40*, 6982−7.
(41) Lee, S.; Antony, L.; Hartmann, R.; Knaus, K. J.; Surewicz, K.; Surewicz, W. K; Yee, V. C. *EMBO J.* **2010**, *29*, 251−62.